Al-Khwarizmi Engineering Journal
ISSN (printed): 1818 – 1171, ISSN (online): 2312 – 0789
Vol. 22, No. 2, June, (2026), pp. 141-152

Al-Khwarizmi Engineering Journal

Levofloxacin Adsorption and Release on γ-Mesoporous Alumina Nanoparticles Using Linear Kinetics Equations

Maryam A. Azeez[1] and Sameer H. Kareem[2*]
[1,2] *Department of Chemistry, College of Science for Women, University of Baghdad, Baghdad, Iraq*
*Corresponding Author's Email: sameerhk_chem@csw.uobaghdad.edu.iq

(Received 10 May 2025; Revised 2 October 2025; Accepted 19 October 2025; Published 1 June 2026)
https://doi.org/10.22153/kej.2026.10.002

Abstract

Mesoporous alumina is a promising drug carrier because of its extensive surface area, pore structure, biocompatibility and non-toxicity, facilitating high drug loading and release capacity. This study aimed to investigate the adsorption and release kinetics of levofloxacin (LF) on prepared γ-mesoporous alumina nanoparticles (γ-MNPs). Adsorption kinetic tests were carried out by a batch method, drug loading was investigated using an impregnation method, and the release kinetics were determined using a dialysis bag maintained at 310 K. Adsorption kinetics were analysed using three kinetics models: the pseudo-first-order, pseudo-second-order and intraparticle diffusion. Results showed that the adsorption of LF followed a pseudo-second-order reaction, with the adsorption rate and mechanisms regulated by two consecutive steps, suggesting that intraparticle diffusion was involved, but it was not the only rate-controlling step. Drug loading results showed that the amount of LF loaded into γ-MNP was 2.17 mg drug/g γ-MNP. The drug release behaviour was investigated at pH 7.4 and pH 5.4. The drug release profile for the LF/γ-MNP system showed that the drug release percentages were 18.00% at pH 5.4 after 48 h and 90.41% at pH 7.4 after 24 h. Drug release was characterised by the kinetic models, including zero-order and first-order kinetics. The data from the pH 5.4 system was best fitted by zero- and first-order kinetics. The drug release mechanisms from a matrix were interpreted using Korsmeyer–Peppas, Kopcha and Higuchi models. The results demonstrated that drug release at pH 7.4 exhibited non-Fickian diffusion, whereas that at pH 5.4 was Fickian diffusion. The Hugichi constants (k_H), which were correlated with the release rate, were low in the two systems, confirming the results of zero- and first-order equations. Therefore, γ-MNP is a promising and effective delivery medium for LF treatment.

Keywords: *Mesoporous alumina; Levofloxacin adsorption; Korsmeyer–peppas model; Levofloxacin loading; Drug release*

1. Introduction

Mesoporous materials, including mesoporous alumina, have recently attracted significant attention because of their high specific area, large pore volume, controlled porosity, chemical inertness and excellent stability [1–3]. Therefore, they are utilised in many applications, including drug delivery systems [4], [5]. In biomedicine, γ-mesoporous alumina is a remarkable matric for extensive drug loading and controlled release (drug delivery) because of its chemical inertness and adjustable surface chemistry [6–8].

Mesoporous alumina, functionalised with various hydrophilic and hydrophobic surface chemical groups, was used as a carrier for the transport of the medication ibuprofen. The incorporation of hydrophobic groups resulted in a rapid release rate (85% over 5 h) and a moderate level of drug loading (around 20%). By contrast, hydrophilic groups yielded reduced release rates (12%–40% over 5 h) and large drug payloads (21%–45%) [9]. The arrangement of functional groups on

the alumina surface and the pore properties of the matrix were shown to influence diffusion-controlled drug release, depending on the chemical moiety. Donepezil hydrochloride, a pharmacological agent for Alzheimer's disease, was administered and released in vitro into artificial cerebrospinal fluid via this method [10]. Additionally, it was used to enhance the administration of pioglitazone in rats with type 1 diabetic nephropathy. The mesoporous material demonstrated a release rate of 80% for pioglitazone, indicating its potential as an effective drug carrier and a platform for the delivery of poorly water-soluble medications to enhance oral bioavailability [11].

Levofloxacin (LF) is a notable member of the quinolone class of antibiotics and is used to treat a wide variety of bacterial infections [12]. A previous study indicated that LF may be repurposed to treat inflammation caused by chronic bacterial infections including cystic fibrosis and pneumonia [13]. Figure 1 illustrates the chemical structure of this drug.

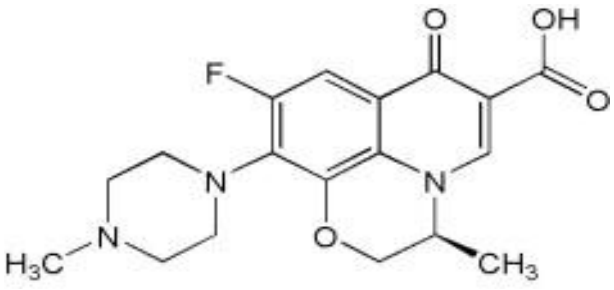

Fig. 1. Chemical structure of LF

A recent study was performed to synthesise mesoporous silica and load it with LF, followed by glycosylation to enhance uptake by bacterial cells. Plain mesoporous silica and glycosylated mesoporous silica nanoparticles exhibited drug loading capacities of 10.41% and 11.43%, respectively. After 48 h, the release of LF from glycosylated silica was 21.02%, whereas that from ordinary silica was 7.50%. The minimum inhibitory concentration of glycosylated silica on *Escherichia coli* was lower than that of plain silica and LF [14]. In vitro release studies of MgO-loaded LF nanoparticles were conducted at 37 °C in simulated bodily fluid. After analysing the data using several kinetic models, researchers found that dissolution is a gradual process requiring 12–24 h to complete [15].

Porous alumina is recognised for its structural integrity, which remains intact under in vitro and in vivo conditions, a notable property that has facilitated its adoption in specialised biomedical applications. Some in vitro immuno-isolation studies carried out in porous alumina membranes suggest that alumina is non-toxic and does not induce significant complement activation. In vitro studies demonstrated the absence of toxic effects from porous alumina capsules. In vivo studies conducted 1 week after implantation revealed moderate inflammation of the tissue surrounding poly(ethylene glycol) capsules [16–18].

A review of existing literature on alumina as a drug carrier reveals a scarcity of studies on the adsorption and release kinetics of drugs, despite the favourable characteristics of alumina, particularly γ-MNP, and the prevalent use of LF and its potential side effects on the body. The present study aimed to investigate the adsorption kinetics of LF by applying different kinetic models. The study also included the release profile and kinetics of LF release after drug loading, using different linear release kinetics equations. According to our knowledge, this study has not been previously addressed.

2. Materials and Methods

2.1. Chemicals

Dioctyl sulfosuccinate sodium salt (AOT, purity 98%) and aluminium nitrate nanohydrate ($Al(NO_3)_3 \cdot 9H_2O$, molar mass 375.134 g/mol, purity 99%) were provided by BDH Chemicals, Ltd., Poole, England. Pharmaceuticals were obtained from the AL-Razi factory in Baghdad.

2.2. Synthesis of γ-Mesoporous Alumina Nanoparticles (γ-MNPs)

The procedure utilised in the synthesis of γ-MNP was as reported in reference [19], with minor modifications as follows: 1.25 g of AOT was dissolved in 100 mL of deionised water (solution A). Subsequently, 11.25 g of $Al(NO_3)_3 \cdot 9H_2O$ was dissolved in 100 mL of distilled water (solution B). Solution B was added to solution A dropwise while stirring for 30 min at 70 °C. The pH of the solution was adjusted to 9 by slowly adding sodium hydroxide (1 M) and agitating, resulting in white suspensions after 120 min at 70 °C. The formed solution was aged in a water bath at 80 °C for 20 h to fully transform into a gel. The products were filtered, rinsed repeatedly with distilled water, dried in an oven set at 80 °C for 8 h and calcined for 4 h at 600 °C.

This γ-MNP was characterised in a previous work [20]. It has a crystalline structure with cubic symmetry; the particle size distribution was in the range of 10–55 nm. The surface area was 319.99 m^2g^{-1}, the pore volume was 0.557 cm^3g^{-1} and the average pore diameter was 6.963 nm.

2.3. Adsorption Kinetic Study

Experiments for adsorption kinetic research were carried out in a 250 mL conical flask that included 0.3 g of γ-MNP and 100 mL of 6 mg/L LF. A water bath shaker operating at 200 rpm was used to agitate the solutions for 180 min at 298 K. Following the interval, the drug concentration was measurable using a UV-vis spectrophotometer by assessing the absorbance at λ_{max} 292 nm.

The amount adsorbed (q_e) was computed using the following equation [21]:

$$qe = \frac{(Co - Ce)V}{m} \quad \ldots(1)$$

where C_o is the starting concentration of the drug, C_e is the equilibrium concentration of the drug, m is the γ-MNP weight and V is the adsorbate solution's volume (L).

2.4. Drug Loading Study

LF was loaded onto the γ-MNP carrier via impregnation. About 15 mL of 50 mg/L drug solution was added to 0.3 g of γ-MNP carrier and placed on a magnetic stirrer for 24 h to achieve equilibrium. The resulting solution was filtered, and the resulting liquid phase was transferred into a quartz cell to determine the amount of LF by using a UV-vis spectrophotometer. Thereafter, the drug-loaded mesoporous composite was dried for 12 h at 50 °C [22], [23].

2.5. In Vitro Release Experiment

The procedure for in vitro release experiments was as follows: a dialysis bag containing drug-loaded γ-MNP with 2 mL of PBS (pH 7.4 or 5.4) was soaked in 18 mL of saline solution and maintained at 37 °C. About 1 mL of sample was extracted at predetermined intervals (replaced with fresh PBS), and the drug concentration in the liquid phase was evaluated using a UV-vis spectrophotometer [22], [23].

3. Results and Discussion

3.1. Characterisation

The carrier after loading with LF (LF γ-MNP) was characterised by XRD, BET, SEM and TGA. Figures 2 displays the XRD patterns of the sample, indicating diffraction peaks at 18.67°, 20.28°, 27.80°, 37.13°, 40.48°, 53.11° and 66.71°. By contrast, γ-MNP before drug loading exhibited diffraction peaks at 39.48°, 45.91° and 66.95° [7], [20].

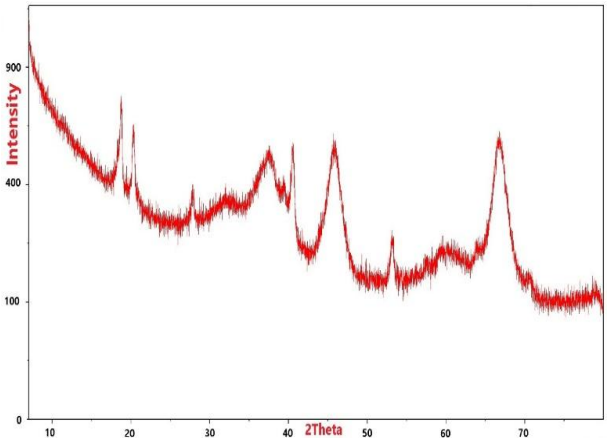

Fig. 2. XRD patterns of γ-MNP after loading with LF

The results of XRD analysis suggested that the chemical formula was $Al_4F_2O_8C_8N_{24}$. The results of the chemical formula and the emergence of peaks at 18.67°, 20.28°, 27.80° and 53.11° may be due to LF loading. BET analysis revealed a reduction in surface area of 6.6 m^2/g (the surface area after drug loading was 313.3 m^2/g), thereby confirming drug loading.

Figure 3 shows the SEM image illustrating that the morphology of LF/γ-MNP consisted of nano-sized particles with irregular agglomeration.

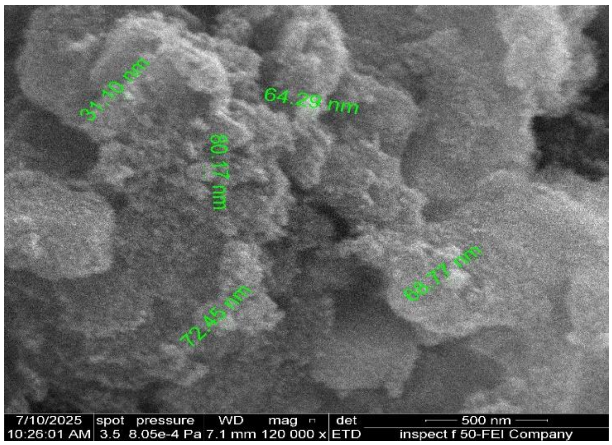

Fig. 3. SEM image (120.000× magnification, scale bar 500 nm) of γ-MNP loading with LF

Figure 4 shows the results of TGA for γ-MNP before and after loading, which was performed in a temperature range from 25 °C to 800 °C. The weight loss for the sample before loading, indicated in one step at 100 °C (Figure 4a), was attributed to the presence of moisture. By contrast, the sample loaded with the drug showed a weight loss in three steps (Figure 4b), indicating moisture loss in the initial step, and the subsequent weight loss in the second and third phases possibly reflect the thermal decomposition of LF. These results confirmed that γ-MNP was loaded with the drug during impregnation.

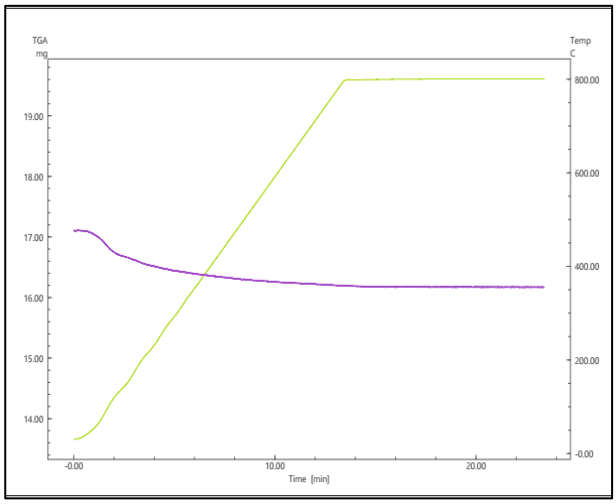

(a)

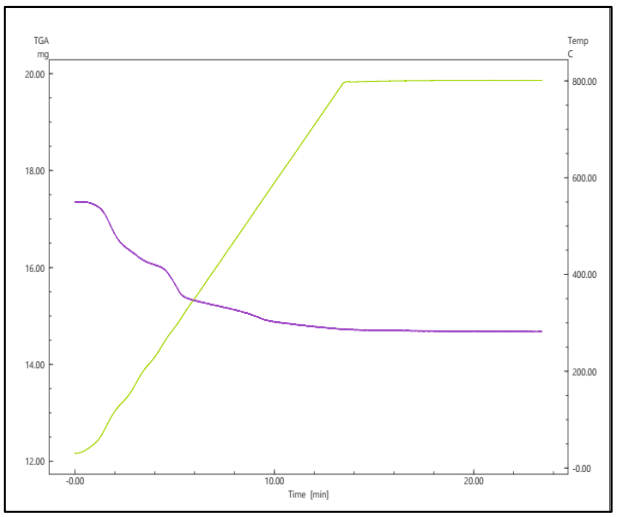

(b)

Fig. 4. TGA spectrum of γ-MNP, a) before and b) after loading with LF

3.2. Adsorption Kinetics

Figure 5 illustrates the results of adsorption kinetic experiments, depicting the fluctuation in the amount of LF adsorbed over time for three concentrations (6, 8 and 10 mg/L) at 298 K.

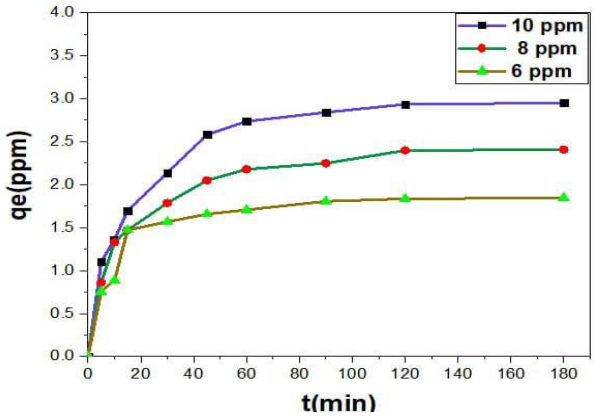

Fig. 5. Variation in q_e with time for the adsorption of three concentrations of LF on 0.3 g of γ-MNP at 298 K

The adsorption behaviour of 6 mg/L LF was investigated using three kinetic models: pseudo-first-order, pseudo-second-order and intraparticle diffusion models. In the pseudo-first-order equation (Lagergren equation), the difference between time-dependent intake (q_t) and equilibrium intake (q_e) is represented as a linear function of adsorption time spent (t), as follows [24], [25]:

$$ln(q_e - q_t) = ln\, q_e - k_1 t \quad \ldots(2)$$

The rate of adsorption was calculated using the following pseudo-second-order equation [26], [27]:

$$t/q_t = 1/k_2 q_e^2 + t/q_e \quad \ldots(3)$$

The Weber–Morris model was applied to delineate the process of diffusion and identify the rate-limiting step [28, 29]. The equation below illustrates this:

$$q_t = k_D t^{1/2} + C \quad \ldots(4)$$

where k_1 is the first-order rate constant, k_2 is the second-order rate constant, k_{D1} and k_{D2} are the diffusion rate constants and C is the plot's intercept.

The linear plots of the three equations are illustrated in Figure 6, which also features a comparative analysis. Table 1 displays all the parameters and regression coefficients obtained from the slope and intercept of the linear plots of the abovementioned kinetic models.

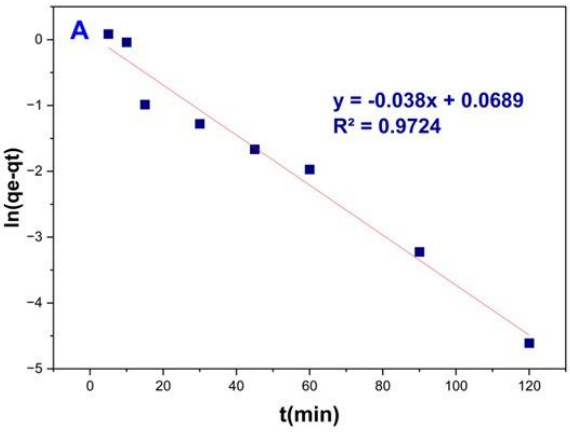

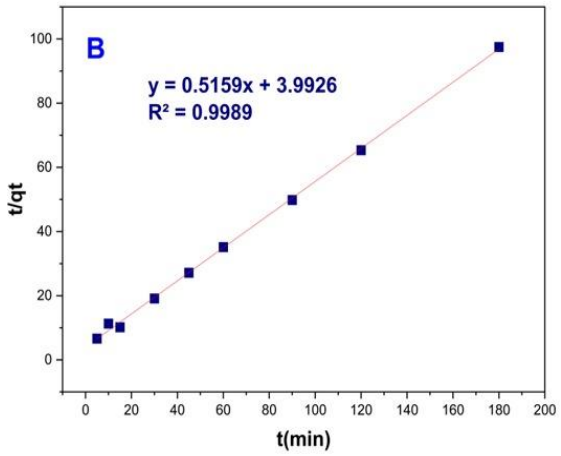

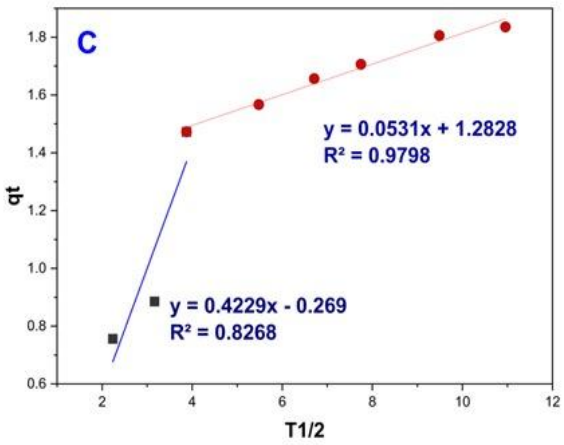

Fig. 6. Linear plots of the A) pseudo-first-order, B) pseudo-second-order and C) intraparticle diffusion kinetic models for LF adsorption on γ-MNP at 298 K.

Table 1,
Kinetic functions of LF adsorption onto γ-MNP at 298 K.

Model	Parameters	Value
pseudo-first-order	q_e (cal) (mg/g)	1.071
	k_1(min)$^{-1}$	0.038
	R^2	0.9724
pseudo-second-order	q_e (cal) (mg/g)	1.938
	k_2 (g/mg·min)	0.0746
	h (mg/g·min)	0.280
	R^2	0.9989
Intraparticle diffusion	K_{D1} (mg/g·min$^{1/2}$)	0.4229
	R_1^2	0.8268
	K_{D2}(mg/g·min$^{1/2}$)	0.0531
	R_2^2	0.9798

Table 1 shows that the pseudo-second-order model was more significant because of its high R^2 (0.9989) and q_e(cal.) (1.938 mg/g) values compared with the other kinetic models. The initial adsorption rate (h) was observed to be 0.28 (mg/g·min), which was calculated using the equation $h = k_2 q_e^2$.

Data were analysed using the intraparticle diffusion model to explore the adsorption mechanism between LF and γ-MNP adsorbent. Finding the potential rate-limiting step in an adsorption process is advantageous. Figure 3C shows that the adsorption rate was controlled by two sequential phases: (i) external diffusion of the adsorbate from the adsorbent surface across the boundary layer and (ii) diffusion through pores or intraparticles. If the plot linearly intersected the origin, then internal diffusion should be the only

factor controlling the adsorption process [30]. The absence of the plot intersecting the origin indicated that intraparticle diffusion was not the only rate-controlling step, but other steps were also involved.

3.3. Release Kinetics of LF

A minimal quantity of drug-loaded carriers may be introduced into a substantial volume of release medium using a dialysis bag to obtain the release profiles of pharmaceuticals. LF was incorporated into carriers for the in vitro assessment of drug release, and the subsequent expression was used to determine the quantity of drug loaded [21]:

$$\text{Loading}\left(\frac{\text{mg drug}}{\text{g sample}}\right) = \frac{(\text{m.orig}) - (\text{m.solu})}{(\text{m .sample})} \quad \ldots(5)$$

where m_{orig} represents milligrams of LF in the solution, m_{solu} denotes milligrams of LF in the solution after impregnation and m_{sample} indicates the grams of the carrier.

The specified amount of LF loaded into the carrier was 2.17 mg of the drug/g carrier. These loading values were consistent with the capacity of other adsorbent drugs defined by previous studies [22], [31],[32]. LF may be incorporated into γ-MNPs via physical entrapment and electrostatic interactions due to the presence of mesopores in the alumina and the Van der Waals forces between the drug and the carrier.

The drug release behaviour was investigated at 37 °C and pH 7.4 and 5.4, simulating physiological conditions. Cumulative LF release is shown in Figure 7.

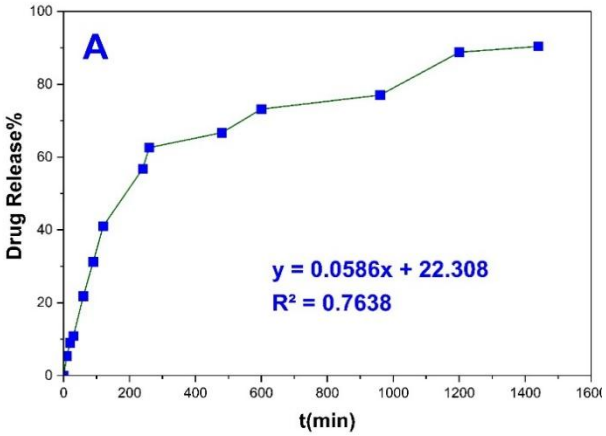

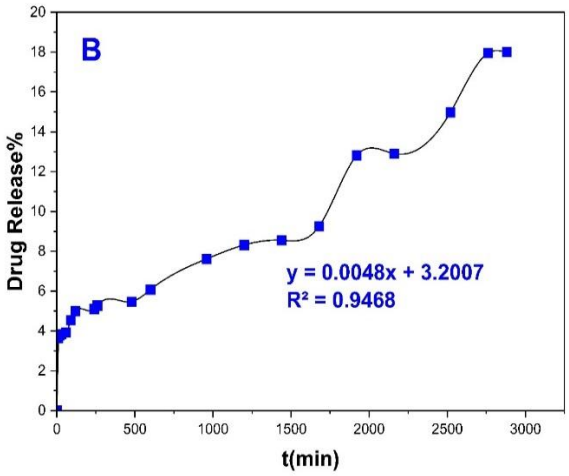

Fig. 7. In vitro release profile of LF-loaded γ-MA at A) pH 7.4 and B) pH 5.4

Figure 6 shows the controlled release curves of LF from LF/γ-MNPs at specific pH levels (pH 7.4 and pH 5.4) over time. LF released from γ-MNP at pH 7.4 exhibited an initial rapid dose, followed by a slow release, reaching 90.41% of loaded LF after 1440 min (24 h). LF released at a low pH (pH 5.4) was relatively slow and reached 18.00% after 2880 min (48 h). These results suggested enhanced adsorption of LF at pH 5.4, which may be due to the pH-dependent chemical structures of LF, predominantly existing in its cationic form at this pH [33]. Thus, the drug release properties of LF/γ-MNP were dependent on pH [34], [35].

The data on LF drug release from the carrier were analysed using five kinetic models: zero-order (Equation 6), pseudo-first-order (Equation 7), Korsmeyer–Peppas (Equation 8), Kopcha kinetics (Equation 9) and Higuchi (Equation 10) [36], [37]:

$$M_t = M_\infty - k_0 t \quad \ldots(6)$$

$$M_t / M_\infty = 1 - e^{(-k_1 t)} \quad \ldots(7)$$

$$M_t / M_\infty = k_{K-p}\, t^n \quad \ldots(8)$$

$$M_t = A t^{1/2} + Bt \quad \ldots(9)$$

$$M_t = k_H\, t^{0.5} \quad \ldots(10)$$

In this case, M_t is the quantity of LF released at time t in minutes; M_∞ is the drug loaded in γ-MNPs; k_0 and k_1 are the zero- and first-order rate constants, respectively; $K_{K\text{-}P}$ and k_H are the kinetic constants associated with the host–guest interaction and Higuchi's release rate constant, respectively; n is the host's form and mechanism of drug release; and k is the first-order rate constant. The linear plots for these models are illustrated in Figures 8 and 9, and the obtained results are listed in Table 2. Figure 8A

illustrates the role of diffusion, and Figure 8B depicts the contribution of erosion.

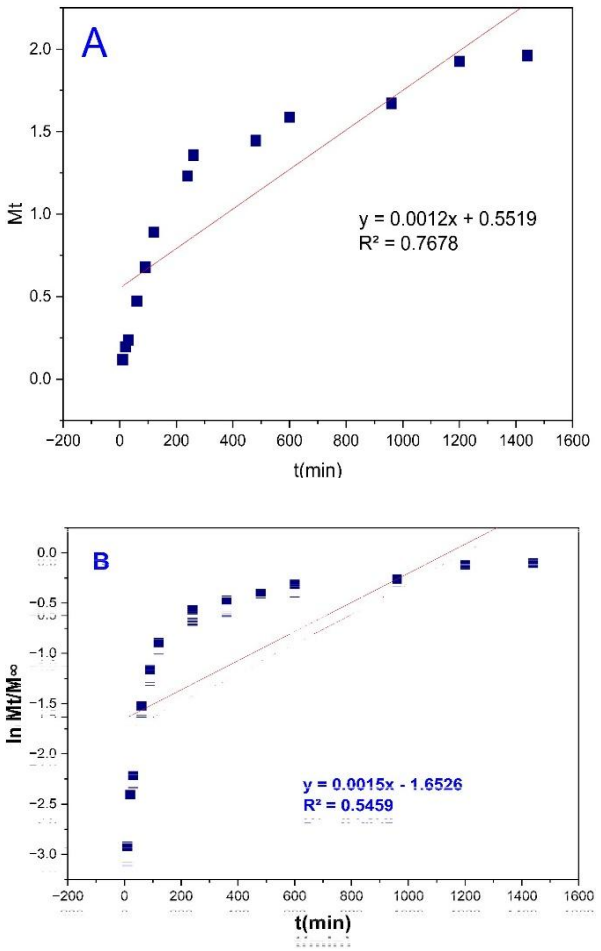

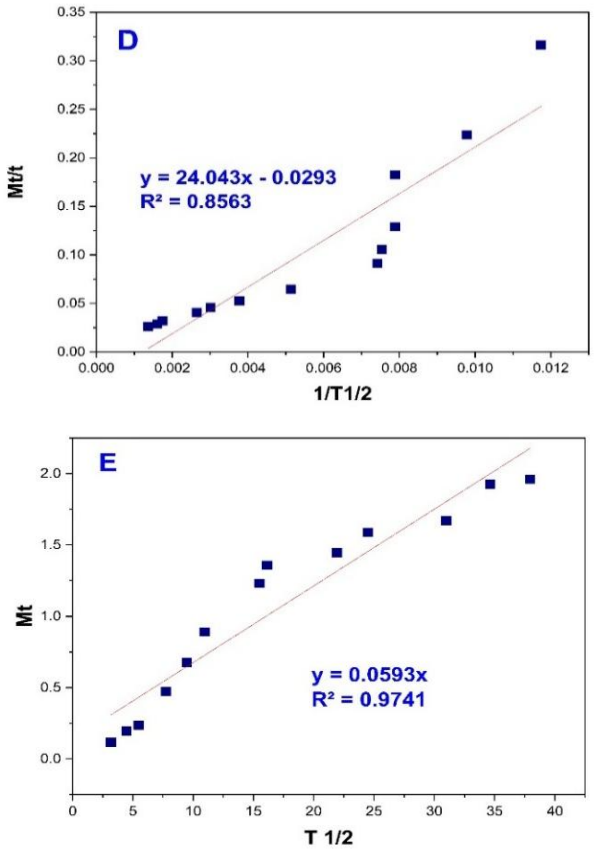

Fig. 8. Linear plots of A) zero-order, B) pseudo-first-order, C) Korsmeyer–Peppas, D) Kopcha and E) Higuchi models of kinetic release from γ-MA after loading with LF at pH 7.4

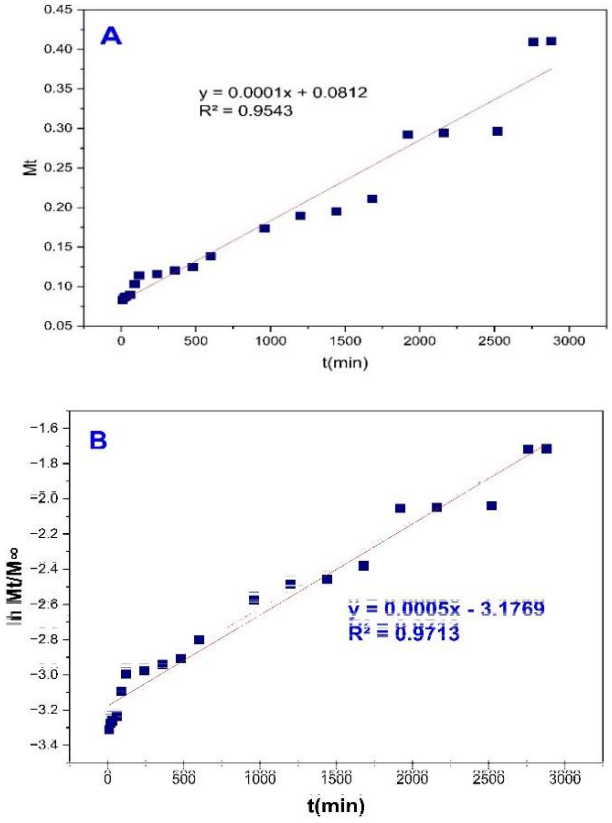

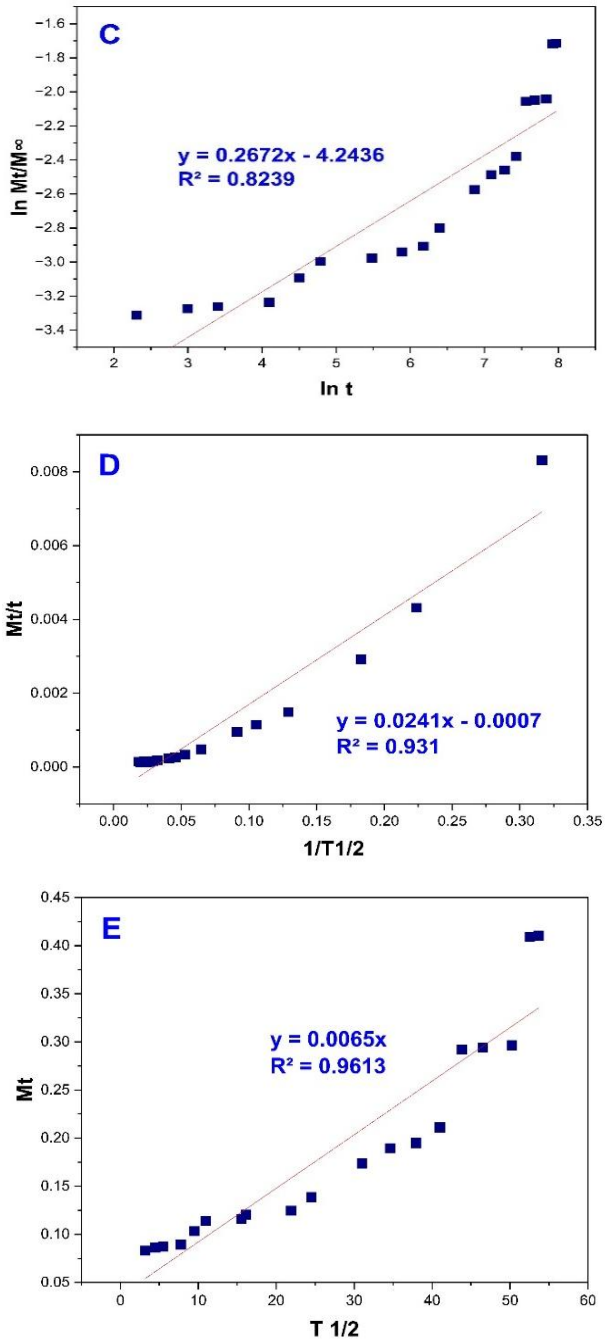

Fig. 9. Linear plots of A) zero order, B) pseudo-first-order, C) Korsmeyer–Peppas, D) Kopcha and E) Higuchi models of kinetic release from γ-MA after loading with LF at pH 5.4.

Drug release from the solid carrier was characterised by the kinetic models, including zero-order kinetics and first-order kinetics. The results in Table 2 showed that the values of R^2 for the two systems were higher at pH 5.4 than at pH 7.4. Thus, the data of the pH 5.4 system were best fitted to zero- and first-order kinetics. The zero-order kinetic dose form is optimal for drug release because it administers a consistent amount of medication over time, leading to a prolonged pharmacological effect [38]. The first-order equation describes the drug release from a system where the release rate is dependent on concentration, and the zero- and first-order equations describe the slow release rate [39].

Table 2,
Kinetic parameters of LF release from LF/γ-MNP at two pH levels and 37 °C.

Model	parameters	pH 7.4	pH 5.4
Zero-order model	k_0	0.0552	0.0048
	R^2	0.7678	0.9468
Pseudo-first-order	k_1	0.0015	0.0005
	R^2	0.9423	0.9457
Korsmeyer–	n	0.5670	0.2670
Peppas model	k_{K-P}	0.0190	0.0143
	R^2	0.9473	0.8239
Kopcha model	A	24.0431	0.0241
	B	0.0293	0.0007
	R^2	0.8563	0.9310
Higuchi model	k_H	0.0593	0.0065
	R^2	0.9741	0.9613

The mechanisms of drug release from a matrix were analysed using the Korsmeyer–Peppas, Kopcha and Higuchi models. For the Korsmeyer–Peppas model, if the release exponent n was ≤ 0.5, the release was dominated by Fickian diffusion; if n was between 0.5 and 1, then the release followed an abnormal diffusion mechanism (non-Fickian diffusion); and if n > 1, the release was based on a complex transport mechanism. The Peppas model exhibited n values of 0.567 and 0.267 for pH 7.4 and pH 5.4, respectively, indicating that the drug release at pH 7.4 was characterized by non-Fickian diffusion, but that at pH 5.4 was characterised by Fickian diffusion. This transition from non-Fickian to Fickian behaviour may be due to the positive charge of the drug at pH 5.4, which may affect the diffusion based on concentration due to electrostatic effects.

In the Kopcha approach, erosion is dominant when A/B < 1, whereas diffusion dominates when A/B ≥ 1. The results showed that the values of A/B for the two systems exceeded 1, demonstrating that diffusion was the predominant mechanism [37, 40]. Higuchi's model revealed the best fit (R^2 =0.974 at pH 7.4 and 0.963 at pH 5.4) indicating that drug release was diffusion at both pH levels. The result of this model also showed that k_H, a constant related to the burst release rate of the release process, was low in the two systems, confirming the results of zero- and first-order equations. This result was confined to other studies [41], [42].

One of the most important limitations of our work was the minimal amount of medicine loaded onto the carrier, which we will address in future studies.

4. Conclusions

The adsorption and release kinetics of LF on γ-MNP demonstrated that the synthesised material was an effective carrier for LF. The investigation of adsorption kinetics showed that the adsorption of LF on γ-MNP completely obeyed the pseudo-second-order equation, with an initial rate of 0.28 mg/g·min, as indicated by a correlation coefficient of R^2=0.9989 and calculated adsorption capacity (q_e(cal)) of 1.938 mg/g. The loading studies demonstrated that γ-MNP possessed a loading capacity of 2.17 mg LF drug/g carrier, with LF release percentages of 90.41% after 1440 min at pH 7 and 18.00% after 2880 min at pH 5 for the LF/γ-MNP system. Drug release was described by the zero-order and first-order kinetic models. The results on the mechanisms of drug release indicated that diffusion was the dominant process. At pH 7.4, drug release exhibited non-Fickian diffusion; at pH 5.4, drug release followed Fickian diffusion. This suggests that the drug adsorption and release properties of LF/γ-MNP were influenced by pH. Further optimisation of the adsorption process parameters, such as pH and carrier functionalisation, may yield superior drug loading capacity and enhance the release profile.

Abbreviations

γ-MNP	γ-Mesoporous alumina nanoparticle
PBS	phosphate buffer solution
LF	levofloxacin
AOT	dioctyl sulfosuccinate sodium salt

Acknowledgements

The authors gratefully acknowledge the staff of the College of Science for Women, University of Baghdad, Iraq.

Conflicts of Interest

The authors declare that there is no conflict of interest regarding the publication of this paper.

References

[1] K. -Xia, S. Hou, Q. Niu, K. Suzuki, and P. Zhang, "Mechanochemical Templated Synthesis of Mesoporous Alumina-Supported Polyoxometalate Catalysts toward Selective Oxidation of Sulfides," RSC Mechanochemistry. 2025,2, 394-398. https://doi.org/10.1039/D4MR00130C.

[2] M. Han et al., "Mesoporous materials 2.0: innovations in metals and chalcogenides for future applications," Bulletin of the Chemical Society of Japan, vol. 98, no. 1, 2025. https://doi.org/10.1093/bulcsj/uoae136.

[3] M. A. Azeez and S. H. Kareem, "Mesoporous γ-Alumina Nanoparticles Synthesis Using Anionic Surfactants as Soft Template and Utilization as Adsorbent for Levofloxacin and Moxifloxacin Drugs," Journal of Nanotechnology, Volume 2025, Article ID 8637079, 13 pages. https://doi.org/10.1155/jnt/8637079.

[4] M. Mirzaei et al., "Silica mesoporous structures: Effective nanocarriers in drug delivery and nanocatalysts," Appl. Sci. (Basel), vol. 10, no. 21, p. 7533, 2020. https://doi.org/10.3390/app10217533.

[5] A. -Mohan et al., "Preparation of melamine-functionalized mesoporous silica nanoparticles for delivery of anticancer drugs," Materials Letters, vol. 371, 2024. https://doi.org/10.1016/j.matlet.2024.136790.

[6] P. F. Fulvio, R. I. Brosey, and M. Jaroniec, "Synthesis of mesoporous alumina from boehmite in the presence of triblock copolymer," ACS Appl. Mater. Interfaces, vol. 2, no. 2, pp. 588–593, 2010. https://pubs.acs.org/doi/10.1021/am9009023.

[7] M. Pourmadadi et al., "Porous alumina as potential nanostructures for drug delivery applications, synthesis and characteristics," J. Drug Deliv. Sci. Technol., vol. 77, no. 103877, p. 103877, 2022. https://doi.org/10.1016/j.jddst.2022.103877.

[8] S. H. Lakade, M. T. Harde, and P. K. Deshmukh, "Synthesis of mesoporous alumina: an impact of surface chemistry on release behavior," Part. Sci. Technol., pp. 1–7, 2019. https://doi.org/10.1080/02726351.2019.1666947.

[9] R. - Shobhna Kapoor and A. J. Hegde, "Influence of surface chemistry of mesoporous alumina with wide pore distribution on controlled drug release," Journal of Controlled

Release, vol. 140, pp. 34–39, 2009. https://doi.org/10.1016/j.jconrel.2009.07.015.

[10] L. -Osama, H. T. Handal, S. A. El-Sayed, E. M. Elzayat, and M. Mabrouk, "Fabrication and optimisation of alumina nanoporous membranes for drug delivery applications: A comparative study," Nanomaterials, vol. 14, no. 13, 2024. https://doi.org/10.3390/nano14131078.

[11] J. Varshosaz, S. Ahmadipour, and A. Dezhangfard, "Mesoporous silica and alumina nanoparticles to improve drug delivery of pioglitazone on diabetic type 1 nephropathy in rats," Res. Pharm. Sci., vol. 19, no. 4, pp. 459–474, 2024. https://doi.org/10.4103/rps.rps_65_23.

[12] A. Lambert, J.-B. Regnouf-de-Vains, and M. F. Ruiz-López, "Structure of levofloxacin in hydrophilic and hydrophobic media: Relationship to its antibacterial properties," Chem. Phys. Lett., vol. 442, no. 4–6, pp. 281–284,2007. https://doi.org/10.1016/j.cplett.2007.05.077.

[13] S. Phuagkhaopong, J. Sukwattanasombat, K. Suknuntha, C. Power, P. Wonganan, and P. Vivithanaporn, "Anti-inflammatory effects of moxifloxacin and levofloxacin on cadmium-activated human astrocytes: Inhibition of proinflammatory cytokine release, TLR4/STAT3, and ERK/NF-κB signaling pathway," PLoS One, vol. 20, no. 1, p. e0317281, 2025. https://doi.org/10.1371/journal.pone.0317281.

[14] R. Mukhopadhyay, S. Narayan, A. Padmaja, S. Shenoy, T. Ashwini, and Y. Usha, "Development of levofloxacin glycosylated mesoporous silica nanoparticles for urinary tract infections," Journal of Applied Pharmaceutical Science, vol. 14, no. 12, pp. 174–179. https://dx.doi.org/10.7324/JAPS.2024.181547.

[15] Abhishek Kumar, R. Rani, P. Dhanda, and K. Sharma, "Synthesis and Characterization of MgO-loaded Levofloxacin Nanoparticles to Combat Salmonella Typhi bacteria," Journal of Chemical Health Risks, vol. 14, no. 4, pp. 1075–1084, 2024. https://www.jchr.org/index.php/JCHR/article/view/5626.

[16] K. E. La Flamme, K. C. Popat, L. Leoni, E. Markiewicz, T. J. La Tempa, B. B. Roman, C. Grimes, T. A. Desai, Biocompatibility of Nanoporous Alumina Membranes for Immunoisolation, Biomaterials 28, 2638, 2007. https://doi.org/10.1016/j.biomaterials.2007.02.010.

[17] E. Xifre-Perez, J. Ferre-Borull, J. Pallares, and L. F. Marsal," Mesoporous alumina as a biomaterial for biomedical applications", Mesoporous Biomater. 2:13–32, 2015. https://doi.org/10.1515/mesbi-2015-0004.

[18] Varshosaz et al.," Mesoporous silica and alumina nanoparticles to improve drug delivery of pioglitazone on diabetic type 1 nephropathy in rats ", Research in Pharmaceutical Science, 19 (4): 459-474, 2024. https://doi.org/10.4103/rps.rps_65_23.

[19] A. A. - Diyarov, N. Q. Mukhamadiev, M. Sayitkulov Sh, and J. R. Uzokov, "Synthesis of mesoporous sorbents on the basis of Al2O3 and their textural characteristics," CAJMNS, vol. 3, no. 3, pp. 511–518, 2022. https://doi.org/10.51699/cajmns.v3i3.817.

[20] M. A. Azeez and S. H. Kareem, "Study of Micellar Behavior of a Tween 80 Surfactant in Aqueous Media Containing Diphenhydramine Hydrochloride", Iraqi Journal of Science, vol. 63, no. 8, pp. 3276–3282, Aug. 2022. https://doi.org/10.24996/ijs.2022.63.8.3.

[21] S. H. Hussein, "Magnetic mesoporous silica material (Fe3O4@ mSiO2) as adsorbent and delivery system for ciprofloxacin drug," in IOP Conference Series: Materials Science and Engineering, vol. 871, IOP Publishing, 2020. https://doi.org/10.1088/1757-899X/871/1/012020.

[22] M. A. Sachit and S. H. Kareem, "Isotherms and thermodynamic parameters of metoprolol drug adsorption on the prepared mesoporous silica," Baghdad Sci. J, vol. 21, no. 3, 2024. https://doi.org/10.21123/bsj.2023.8827.

[23] S. S. -Imam, S. N. Bukhari, J. Ahmad, and A. Ali, "Formulation and optimization of levofloxacin loaded chitosan nanoparticle for ocular delivery: In-vitro characterization, ocular tolerance and antibacterial activity," International Journal of Biological Macromolecules, vol. 108, pp. 650–659, 2018. https://doi.org/10.1016/j.ijbiomac.2017.11.170.

[24] S. Y. - Lagergren, "Zur theorie der sogenannten adsorption geloster stoffe. 1st Edn," in Kungliga Svenska Vetenskapsakademiens, Handlingar, 1898.

[25] I. H. Ali and S. H. Kareem, "Interfacial interaction of binary mixtures of surfactants hexadecyl benzylammonium chloride (HDBAC) and Tween 20 in aqueous solutions," J. Surf. Sci. Technol., 35(3-4), 114–

119. 2020. https://doi.org/10.18311/jsst/2019/21455.
[26] Y. S. Ho and G. McKay, "Pseudo-second order model for sorption processes," Process Biochem., vol. 34, no. 5, pp. 451–465, 1999. https://doi.org/10.1016/S0032-9592(98)00112-5.
[27] I. H. Ali, , A. H. Hamed;, E. Abdul Hussein; and, S. A. Dhahir. "Hydrothermal synthesis of high surface area mesoporous silica as an efficient adsorbent for removal of crystal violet dye from aqueous solution," Baghdad Science Journal: (2025) Vol. 22: Iss. 8, Article 7. https://doi.org/10.21123/2411-7986.5018.
[28] W. J. Weber Jr and J. C. Morris, "Kinetics of adsorption on carbon from solution," J. Sanit. Eng. Div., vol. 89, no. 2, pp. 31–59, 1963. https://doi.org/10.1061/JSEDAI.0000430.
[29] A. V. Dolganov, E. E. Muryumin, O. Y. Chernyaeva, E. A. Chugunova, V. P. Mishkin, and K. N. Nishcev, "Fabrication of new metal-free materials for the hydrogen evolution reaction on base of the acridine derivatives immobilized on carbon materials," Mater. Chem. Phys., vol. 224, pp. 148–155, 2019.https://doi.org/10.1016/j.matchemphys.2018.12.006.
[30] I. Bhogal, K. Mohiuddin, K.-H. Kaur, and A. K. Kim, "Mesoporous silica imprinted nanocomposites for selective adsorption and detection of levofloxacin," Journal of Water Process Engineering, vol. 57, 2024. https://doi.org/10.1016/j.jwpe.2023.104693.
[31] P. Singh, P. K. Maiti, and K. Sen, "Pristine and modified-mesoporous alumina: molecular assistance-based drug loading and sustained release activity," Bull. Mater. Sci. (India), vol. 43, no. 1, 2020. https://doi.org/10.1007/s12034-019-1991-1.
[32] N. Safaran et. al," Advances in polymeric and non-polymeric nanocarriers for the magnified delivery of levofloxacin against bacterial infection", J Nanopart Res, 26:190, 2024. https://doi.org/10.1007/s11051-024-06087-z.
[33] H. Mohammed, S. Al-Jabari, S. Sulaiman, R. Ali, A. Barakat, and A. Safyan, "Adsorption study of levofloxacin on reusable magnetic nanoparticles: Kinetics and antibacterial activity," Journal of Molecular Liquids, vol. 291, 2019. https://doi.org/10.1016/j.molliq.2019.111249.
[34] R. A. -Balaji, S. Raghunathan, and R. R. Levofloxacin, "Levofloxacin," Egyptian Pharmaceutical Journal, vol. 14, no. 1, pp. 30–35, 2015. https://doi.org/10.4103/1687-4315.154705.
[35] L. É. Uhljar, S. Y. Kan, N. Radacsi, V. Koutsos, P. Szabó-Révész, and R. Ambrus, "In vitro drug release, permeability, and structural test of ciprofloxacin-loaded nanofibers," Pharmaceutics, vol. 13, no. 4, p. 556, 2021. https://doi.org/10.3390/pharmaceutics13040556.
[36] I. S. Bayer, "Controlled drug release from nanoengineered polysaccharides," Pharmaceutics, vol. 15, no. 5, p. 1364, 2023. https://doi.org/10.3390/pharmaceutics15051364.
[37] W., Zhu; Long, J.; Shi, M." Release Kinetics Model Fitting of Drugs with Different Structures from Viscose Fabric", Materials, 16, 3282, 2023. https://doi.org/10.3390/ma16083282.
[38] O. Chime Salome and O. Godswill, "Kinetics and Mechanisms of Drug Release from Swellable and Non Swellable Matrices: A Review," RJPBCS, vol. 4, 2013. https://www.rjpbcs.com/pdf/2013_4(2)/[10].
[39] A. Kumar, A. Soni, A. Kumar, Yashpal, and J. Devi, "Preparation of Luliconazole loaded silver nanoparticles Topical gel," J. Drug Deliv. Ther., vol. 12, no. 4, pp. 31–35, 2022. http://dx.doi.org/10.22270/jddt.v12i4.5424.
[40] B Shree Haripriya, D. R. Anakha, R. Yamuna, M. Vinoba, and M. Bhagiyalakshmi, "Green synthesized AgNPs using Clitoria ternatea extract and its confinement on SBA-15/GPTMS-TAEA for controlled drug release of ciprofloxacin," J. Porous Mater, vol. 31, no. 1, pp. 351–363, 2024. http://dx.doi.org/10.22270/jddt.v12i4.5424.
[41] H. -Kapoor, M. Aqil, S. S. Imam, Y. Sultana, and A. Ali, "Formulation of amlodipine nano lipid carrier: Formulation design, physicochemical and transdermal absorption investigation," J. Drug Deliv. Sci. Technol, vol. 49, pp. 209–218, 2019. https://doi.org/10.1016/j.jddst.2018.11.004.
[42] K. Jindal, "RSM-CCD optimized microwave-assisted synthesis of chitosan and sodium alginate based nanocomposite containing inclusion complexes of β -cyclodextrin and amlodipine besylate for sustained drug delivery systems," J. Drug Deliv. Sci. Technol, 2021. https://doi.org/10.1016/j.jddst.2021.102325.

أمتزاز وإطلاق الليفوفلوكساسين على جسيمات نانوية من γ - الومينا متوسطة المسامية : التحليل باستخدام معادلات حركية خطية

مريم عبد الامير عزيز[١] و سمير حكيم كريم[٢]*

[٢،١] قسم الكيمياء، كلية العوم للبنات، جامعة بغداد، العراق

*البريد الالكتروني: sameerhk_chem@csw.uobaghdad.edu.iq

المستخلص

تم التحقيق في حركية الامتزاز والاطلاق لدواء الليفوفلوكساسين (LF) على جسيمات نانوية من الألومينا متوسطة المسام (γ-MNP) وتم تحضيرها مسبقا. أجريت تجارب دراسة حركية الامتزاز بطريقة الدفعات، بينما أجريت دراسة حركية الإطلاق باستخدام (dialysis bag) عند ٣١٠ كلفن. تم إجراء تحليل حركية الامتزاز باستخدام ثلاثة نماذج حركية: الرتبة الكاذبة الأولى والرتبة الكاذبة الثانية والانتشار داخل الجسيمات. اظهرت النتائج أن امتزاز دواء LF هو من الرتبة الكاذبة الثانية، وان الامتزاز وآلياته قد تم من خلال خطوتين متتاليتين: الانتشار الخارجي وانتشار المسام، واظهرت أن الخطوة المحددة للسرعة هي الامتزاز داخل الجسيمات بالاضافة الى خطوات اخرى كون ان الخط المستقيم لم يمر من نقطة الأصل. تم التحقق في تحميل الدواء باستخدام طريقة التشرب وأظهرت النتائج أن كمية LF المحملة في γ-MNP كانت ٢,١٧ ملغم دواء لكلّ غرام γ-MNP. تم التحقيق في سلوك إطلاق الدواء عند pH = ٧,٤ و ٥,٤ ويظهر شكل إطلاق الدواء لنظام LF / γ-MNP أن نسبة إطلاق الدواء بعد ٤٨ ساعة كانت حوالي ١٨,٠٠ ٪ عند pH ٥,٤ ، بينما كانت نسبة إطلاق الدواء بعد ٢٤ ساعة حوالي ٩٠,٤١ ٪ في pH ٧,٤. درس إطلاق الدواء أيضًا باستخدام النماذج الحركية من الدرجة الصفرية والدرجة الأولى وتشير النتائج إلى أن بيانات pH ٥,٤ كانت أفضل ملاءمة للرتبة الصفر و الأولى. تم تفسير آليات إطلاق الدواء باستخدام نماذج Korsmeyer-Peppas و Kopcha و Higuchi. أظهرت النتائج أن إطلاق الدواء عند الرقم الهيدروجيني ٧,٤ كان انتشارًا من نوع (non-Fickian) ، وعند الرقم الهيدروجيني ٥,٤، كان الإطلاق انتشارًا من نوع (Fickian)، وإن سرعة الإطلاق منخفضة في النظامين، مما يؤكد نتائج معادلات من الرتبة الصفر والدرجة الأولى.